Undergraduate Theses   **Honors College**

2021

Utilizing Acoustic Levitation to Determine Ionic Liquid Effects on Enthalpy of Polymerization

Davina V. Ho
University of South Alabama

University of South Alabama

JagWorks@USA

Undergraduate Theses

Honors College

2021

Utilizing Acoustic Levitation to Determine Ionic Liquid Effects on Enthalpy of Polymerization

Davina V. Ho
University of South Alabama

Follow this and additional works at: https://jagworks.southalabama.edu/honors_college_theses

Part of the Other Medical Sciences Commons

Recommended Citation

Ho, Davina V., "Utilizing Acoustic Levitation to Determine Ionic Liquid Effects on Enthalpy of Polymerization" (2021). *Undergraduate Theses* . 18.
https://jagworks.southalabama.edu/honors_college_theses/18

Utilizing Acoustic Levitation to Determine Ionic Liquid Effects on Enthalpy of Polymerization

By

Davina V. Ho

A thesis submitted in partial fulfillment of the requirements of the University of South Alabama

Honors College and the Bachelor of Sciences degree in Biomedical Sciences.

University of South Alabama
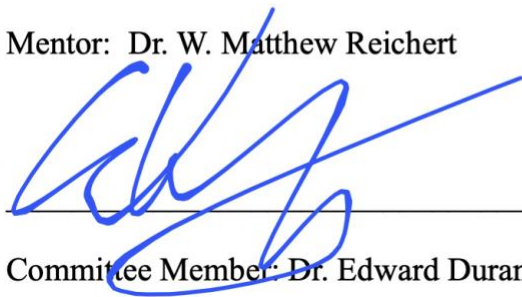
Mobile, Alabama

April 2021

Approved by:

_____
Mentor: Dr. W. Matthew Reichert

_____
Committee Member: Dr. James Davis Jr.

_____
Committee Member: Dr. Edward Duranty

_____
Honors College Dean: Dr. Kathy Cooke

I would like to dedicate this work to my parents, Lily and Mike Ho, as well as to my grandparents, Mỹ Vân and Oai Vũ, who have given me the utmost support and encouragement throughout the years. Without the help and connections of my parents, I would have never had the opportunity to begin researching with my mentor, Dr. Reichert, starting all the way back in high school. They have always stressed the importance of hard work, dedication, and passion— all of things required to help me finish my undergraduate honors thesis. Thank you for exposing me to so many different areas in high school where I was able to learn more about myself such as my likes, dislikes, and ultimately where my passions lie. I am forever grateful that you helped foster my curious, growth mindset and taught me to never stop asking questions, to always figure out the "why" to things, and to use obstacles as learning opportunities. These skills are the foundation of a successful researcher, and I attribute much of my success to my parents as well as my mentor.

ABSTRACT

Ionic liquids (ILs) are emerging as an eco-friendlier alternative to traditional organic compounds. The hope with ILs in this project is to incorporate them with resins used in 3D printing to act as plasticizers which will in turn help prolong the life of the printed object. A common issue with plasticizers like phthalate in particular is they can leach out of plastics due to their vapor pressure which leads to decreased performance and can also pose a health risk being released into its surroundings or atmosphere. A major benefit of incorporating ILs in with resins comes from their low volatility which allows it to remain in the plastic and can prevent the printed object from becoming prematurely brittle. In order to move forward in attempting to integrate ILs in with resin, one needs to understand what effect it has on the heat capacity and polymerization of the resin when combined is the next step. A possible means to study this effect is by measuring the change in temperature of a reaction that is container-less which can be accomplished through acoustic levitation. The aim for this research is to levitate droplets of ILs and methyl methacrylate-based resin in an acoustic levitator, expose the droplet to lasers in order to induce photoinitiated polymerization, and record the temperature change using a FLIR camera. Coupling this data with heat capacity measurements from the DSC will allow us to calculate the heat of polymerization of PMMA and to observe how different concentrations of IL affect the heat capacity and heat of polymerization.

TABLE OF CONTENTS

Page

LIST OF ABBREVIATIONS

IL: Ionic liquid

MMA: Methyl methacrylate

PMMA: Poly (methyl methacrylate)

UV: Ultraviolet

[Bmim][Tf$_2$N]: 1-butyl-3-methylimidazolium bis(trifluorosulfonyl)imide

[Emim][Ace]: 1-ethyl-3-methylimidazoium acetate

BAPO: Phenylbis(2,4,6-trimethylbenzoyl) phosphine oxide

DSC: Differential scanning calorimetry

TGA: Thermogrametric analysis

CSV: Comma separated value

LIST OF FIGURES

CHAPTER 1

INTRODUCTION

I. Ionic Liquids

The exact definition of an ionic liquid (IL) has been up for debate since the field was established as distinctly different from molten salts. For the purposes of this discussion, ILs are organic salts that melt below 100°C.[1] The chemical, physical, and thermal properties of ILs can vary depending on the ions used which allows for potential uses in a variety of applications. Some of these properties include low vapor pressure/low volatility at ambient temperatures, controllable melting points, wide range of viscosity, great solubility for a variety of substances, a larger range of thermal stability, controllable polarity, and can be non-flammable.[2] These physical properties of ILs vary depending on cation and anion structure. The properties can be controlled through manipulation of the alkyl chain lengths of the groups on the cation, the structure of the cation and/or anion, and the functional groups on the cation or anion.[3] ILs could play a key role in the search for an efficient, green eco-friendly alternative to the commonly used volatile organic solvents[4]. Because of their nonvolatility, they do not emit any vapors, this allows for ILs to be used as plasticizer thereby staying in the printed object much longer than traditional plasticizers, ultimately prolonging the life of that object. Plasticizers help increase flexibility and plasticity of materials they are added into.[3]

There are approximately around 300 to 400 kinds of commonly used organic solvents while statistical predictions have estimated that the number of ILs could be 10^8 due to different cation/anion combination.[5] Some common applications of ILs today include separation technology, catalysis, nanoparticle synthesis, and materials and surface sciences such as being able to control surface wettability by simple anion exchange.[5] ILs can also be seen as a better

mechanical lubrication alternative to commercial products due to their unique dipolar structure and their ability to be easily absorbed on sliding surfaces. Another exploratory use of ILs currently is in fuel desulfurization because the IL acts as the extractor; by using a specific IL it was shown that the sulfur concentration in gasoline could possibly be reduced up to 37%.[5]

The leading plasticizer on the market currently is dioctyl pthalate (DOP) accounting for more than 50% of all plasticizing agents used in the formulations of polymers. A few issues arise with traditional plasticizers such as their inadequate thermal stability and tendencies to leach out into the surroundings further causing environmental and health concerns. One example for a need of stability with a wide range in temperatures would be in the case of space applications where an object in space could be facing or shielded from the sun. This is where ILs would be ideal to use as a plasticizer because with their wide temperature range, they remain liquid. On the issue of leaching, one of the biggest concerns is that phthalates could potentially leach out from medical tubing into biological fluids such as blood causing even bigger issues. A major advantage of ILs is their versatility and ability to be chemically designed and specifically tailored to be a solution for niche issues such as this.[6]

One use of ILs that is becoming more important is their role in polymerization processes. Due to their ionic nature, ILs are highly polar which can prove useful in acting as a solvent particularly in radical polymerization. Shown in a study using the Pulse Laser Polymerization technique, that the methyl methacrylate propagation rate constant increases when polymerization occurs in IL and while not only the rate of polymerization increased but the molecular weights of the polymers in comparison to polymerization in just a benzene solution did as well.[7] Another benefit in addition to ILs acting as a plasticizer for poly(methyl methacrylate) is that they can be

recycled easily since they are soluble in some organic solvents but immiscible in others via tuning the cations and anions.[7]

Looking further into IL interaction with PMMA, it has been experimentally shown that the plasticizer's steric hinderance increases the average space in between polymer chains as well as prevents crosslinking.[8] PMMA is commonly used in additive manufacturing which is useful to rapidly and precisely print a plethora of shapes at an affordable cost. By incorporating ILs into the resin used for stereolithography, the printed object should possess characteristics of the embedded IL. AM is more advantageous than methods in which a bulk amount of material is polymerized and then shaped down into the final product because it produces less waste and requires less energy. In order to change the properties of the printed material additives such as plasticizers are incorporated in with the polymer which has become a very common practice in the manufacturing of polymers.[8]

II. Polymerization of PMMA

Recently, polymers are used in a magnitude of spheres of our everyday life. It is said that "polymer forms the backbone of modern society."[9] Polymers are simply large molecules made up of covalently linked smaller molecules (monomer units) The term "polymer" itself is derived from the Greek words *polys* which means "many" and *meros* which means "parts"[9]. For many decades, polymers have been used in industrial bulk materials as well as gaining traction in technological fields such as nanotechnology also.[9]

In general, there are two major types of polymerization—chain-reaction (addition) polymerization, and step-reaction (condensation) polymerization.[9] A visual break down of polymerization and its subcategories can be seen in Figure 1.
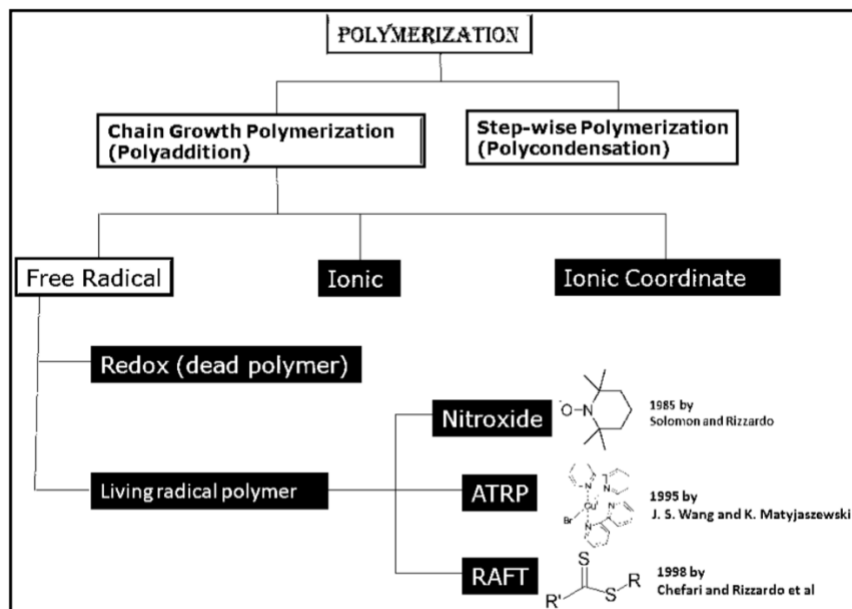
Figure 1. A general breakdown of different types of polymerization.[9]

Anionic polymerization is an example of addition polymerization and is also coined a "living polymerization" which essentially means that the polymer chain that is growing is not terminated. The monomers that are able to form a stable carbanion species when undergoing polymerization are the ones susceptible to anionic polymerization. (Meth)acrylates and especially styrene and its derivatives, for example, are typically successful in undergoing anionic polymerization.[10] One of the benefits for anionic polymerization is that the living anionic polymers have chain-end anions. Under certain conditions, these chain-end anions are highly reactive but still stable. This property is ideal for the synthesis of various branched and linear macromolecular architectures.[10] This living anionic polymerization has a prominent role in industry because it is used to produce a variety of industrial material such as polystyrene, a thermoplastic elastomer which has the potential for processability and elasticity. Figure 2 depicts the general mechanism for the living anionic polymerization of styrene with protection.[11]

F: functional group, (F): protected form of functinal group
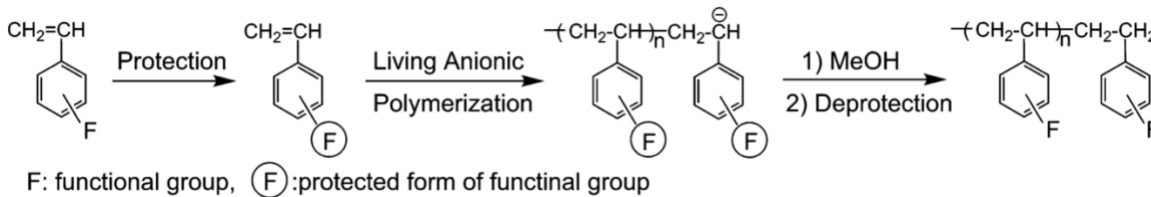
Figure 2. The mechanism for anionic polymerization of styrene.[12]

Due to the repulsion of similar charges, the chain ends are "living", or not easily terminated without addition of a new species, allowing for perfect control of the molecular architecture in anionic polymerization. However, some drawbacks to using anionic polymerization include extreme reactivity with even the smallest traces of water, oxygen, or carbon dioxide with the carbanion and also not being able to perform anionic polymerization under high reaction temperatures.[13]

Another common form of polymerization is free-radical polymerization. Within this category of polymerization are different methods as to how the radical polymerization is initiated. For thermally initiated free-radical polymerization, the addition of an initiator is not needed to form radicals but once the reactive species is formed, the typical mechanism of free radical polymerization can proceed.[12]

A different form of free-radical polymerization is photoinitiated free-radical polymerization. Unlike being initiated solely by heat, this method requires the presence of an initiator and then a light source that forms free radicals, such as UV lasers like those used in this work. The application of this type of technique has varied from curing acrylate dental fillings and 3D printing of objects. A benefit of photoinitiation is that these polymerization reactions can take place in room temperature or lower. Another difference is that unlike thermal initiation, there are fewer side reaction that occur such for photopolymerization. With thermal initiation, the probability for chain transfer to occur is much higher causing more branched macromolecules.[14]

Azobisisobutyronitrile (AIBN) and benzoyl peroxide (BPO) are two very commonly used free-radical initiators for this method of polymerization.[13] The main advantage of using photoinitiated polymerization is control because the light source can be turned on or off to quickly start or stop the process.
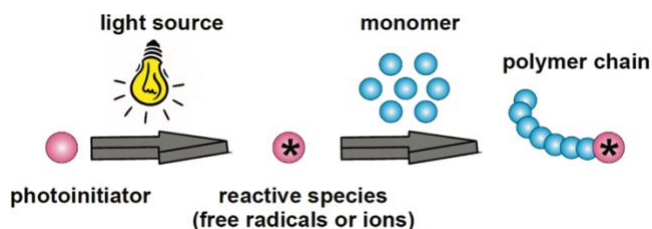
Figure 3. The general mechanism for photoinitiated free-radical polymerization.[14]

Briefly, free-radical polymerization works is when an active species is formed (a radical) due to the decomposition of an initiator molecule causing the first initiation step (I → I*); then this initiator fragment goes on to react with monomer (M) to begin the process of creating a polymer (P) where the center of this activity remains in the adduct. Monomers are then continually added on in this manner with the radical moving from one monomer unit down to the next at the end until termination happens (I*+ M→IM*+M → IMM*…P_i*). Finally in termination, usually two polymers that have active centers will combine so that the active center is now deactivated and the final polymer consists of the two chains linked together (P_i* +P_j* → P_{i+j}). This can be further depicted by Figure 4 of the basic mechanism for free-radical polymerization of methyl methacrylate. An issue with this method of polymerization is that there is difficulty controlling the molecular weight and weight distribution of the polymer. The interaction between radical chains happens very rapidly in contrast to ionic polymerization.[13] This means that it is more difficult obtain polymers that have a predetermined functionality along with well-defined

6

copolymers. One of the benefits of free-radical polymerization is that there is more flexibility with the reaction condition for example having tolerance for trace amounts of impurities.[9]
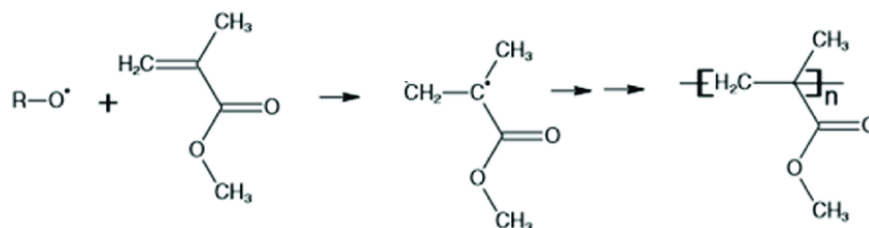
Figure 4. The mechanism for free-radical polymerization of methyl methacrylate monomer to PMMA.

III. Acoustic Levitation

Acoustic levitation creates standing sound waves that allow objects to be suspended in mid-air. The first ever use of acoustic levitation dates back to 1933 when Bücks and Müller used this method to levitate droplets of ethanol between a reflecting wall and vibrating rod.[15] Acoustic levitation since then has evolved and proved very useful with applications that range from common experiments such as acid/base titrations, liquid/liquid extractions and solvent exchanges, to contactless transportation, and even manipulating and mixing samples of DNA plasmids and living cells.[15,16] From these applications, there are a variety of benefits for why this method of acoustic levitation would be preferred. A few of these benefits include "preventing the chemical and thermal contamination that accompanies contact between drops and external objects… [and] the added advantage of increased sensitivity of detection, since no walls disturb detection."[16] While there is no thermal contamination and also no analyte adsorption at container walls, there are other things that need to be considered such as interaction with the surrounding atmosphere as well as the evaporation of solvent.[17]

7

The theory behind how acoustic levitation works is when two waves of the same frequency are coming from opposite directions which creates standing waves where they combine to form a constructive and destructive interference pattern. The points in which the standing wave is experiencing destructive interference along the reflected wave are referred to as "nodes."[18] For the areas of destructive interference, the space between the molecules has lower density and is larger meaning there are fewer molecules moving in and out of the node causing lower pressure. Because sound propagates as a pressure wave, a shift in the distribution of molecules is caused in the medium in which the wave is traveling due to the sound waves. The space between the molecules become smaller in the areas of constructive interference so therefore allows more molecules to move into and out of the "anti-node" ultimately increasing the pressure within that space. The figure below shows a visual representation of standing waves and potential setups of different acoustic levitators.
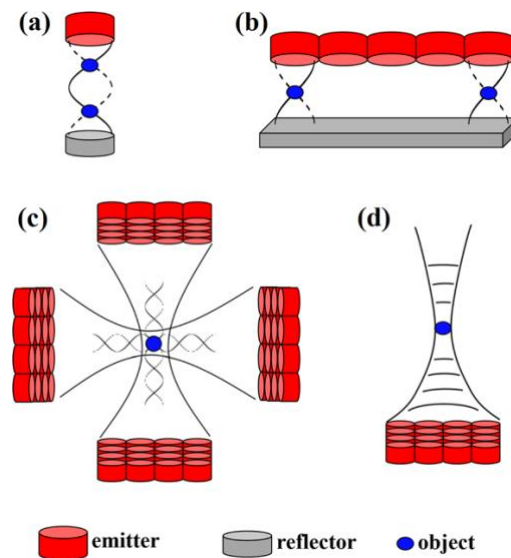

Figure 5. "Schematic of different types of acoustic levitators. (a) Single-axis acoustic levitator. (b) Two-dimensional manipulation of multiple drops using an array of Langevin-type transducers and an opposing reflector. (c) Three-dimensional manipulation of levitated particles using four orthogonal arrays of ultrasonic emitters. (d) Single-beam trapping."[15]

With this technique does come some limitations though. Since the nodes of these standing waves are so low pressure, these areas are only capable of measuring half of the wavelength of that standing wave, meaning acoustic levitators are only able to levitate objects that have diameters smaller than that. Another limitation is the acoustic levitator is only capable of levitating objects that weigh less than the wave's maximum pressure because the pressure is produced must be able to counteract the force of gravity being exerted on the suspended object.[18] In order to physically and logistically be able to create these standing waves, transducers are needed for converting electrical energy into sound. Generally, curved reflector setups are used because it allows for a more focused and localized pressure on the object that is being levitated.[18]

Keeping in mind the potential applications of ILs, the relevance of polymers and polymerization today, and new-found applications of acoustic levitators, being able to record the change in temperature of a suspended polymerization to calculate enthalpy could be revolutionary. With the proposed set up for this project, the hope is to be able to more accurately measure the change in temperature from the heat that the polymer is releasing to the solvent surrounding it which is the monomer and IL for this project. If a traditional method was used, extra heat would be lost to the reaction vessel so by performing the entire polymerization reaction in mid-air, the direct heat given off to the solvent allows for a more accurate representation of the actual heat being released from the reaction.

Thermography was used in order to capture the temperature changes in during the polymerization reaction via FLIR One Pro Camera. This non-contact device detects thermal energy, or heat, and converts it into a thermal image. The temperature of the designated spot can be recorded each second to determine the change in temperature throughout the whole reaction.

CHAPTER 2

HYPOTHESIS

Our hypothesis is that it is possible to use the acoustic levitation/FLIR camera technique to calculate the heat of polymerization of PMMA and observe the effects ILs have on the heat of polymerization.

CHAPTER 3

PURPOSE

With the rising popularity of 3D printing and emergence of new applications of ILs, a new set of questions to navigate transpires. In order to one day incorporate ILs in plastics on a bulk scale, the effects of heat capacity and heat of polymerization of varying amounts of IL in the resin must be discovered and understood. If the effects are successfully studied via this novel acoustic levitation method, this could open up possibilities for more environmentally friendly, durable, and long-lasting plastics.

CHAPTER 4

EXPERIMENTAL METHODS

I. Materials

The chemicals used include methyl methacrylate, 99% purity (Spectrum Chemical MFG Corp – Gardena, California); styrene, 99.% purity (Acros Organics from Fisher Chemical – Waltham, Massachusetts); ethyl acetate, 99.5% purity (Fisher Chemical – Waltham, Massachusetts); methylene chloride, 99.99% purity (Fisher Chemical – Waltham, Massachusetts); phenylbis(2,4,6-trimethylbenzoyl) phosphine oxide, 97% purity (Sigma-Aldrich – St. Louis, Missouri); 2,2'-Azobis(2-methylpropionitrile), 98% purity (Sigma-Aldrich – St. Louis, Missouri). All chemicals were used as received unless stated otherwise. Other materials used include clear V4 photopolymer resin 1L (FormLabs – Somerville, Massachusetts) and silica gel with a pore size of 60 Å, 200-425 mesh particle size, >99% purity (Sigma-Aldrich – St. Louis, Missouri).

II. Construction of the BigLev

The Acoustic Levitator kit instructions were followed from the instructables website with minor modifications.[19] First, the BigLev half stl file was downloaded in order to 3D print the two halves via Formlabs Form 2 SLA 3D printer with the commercial clear v04 PMMA resin. A 6 mm hole was drilled in the center of each of the two pieces to allow for two separate 405nm lasers to shine through. The two halves of the base were then attached together to using epoxy glue and left to set up and dry. The polarity of the 16-millimeter diameter kHz transducers was quantified using a multimeter and then the legs were marked to ensure they were correctly glued into the base oriented with the same polarity. A little dab of hot glue was applied to each

transducer then glued into sockets making sure the marked legs of the transducers were pointing inward toward the center facing the hole for the laser. Next, copper wire was used to make concentric rings around the legs of the transducers and soldering all the pins to the copper wire circle. Black and red long wires were prepared and soldered to the transducers with the black and red wires being attached to alternating copper rings. The wiring from the instructables was followed to ensure the signal emissions were synchronized. The power supply used was the KORAD KA3005d Digital Control DC Power Supply. The BigLev was then attached upright to a ring stand using clamps along with two UV lasers positioned to shine through the holes drilled in the BigLev.
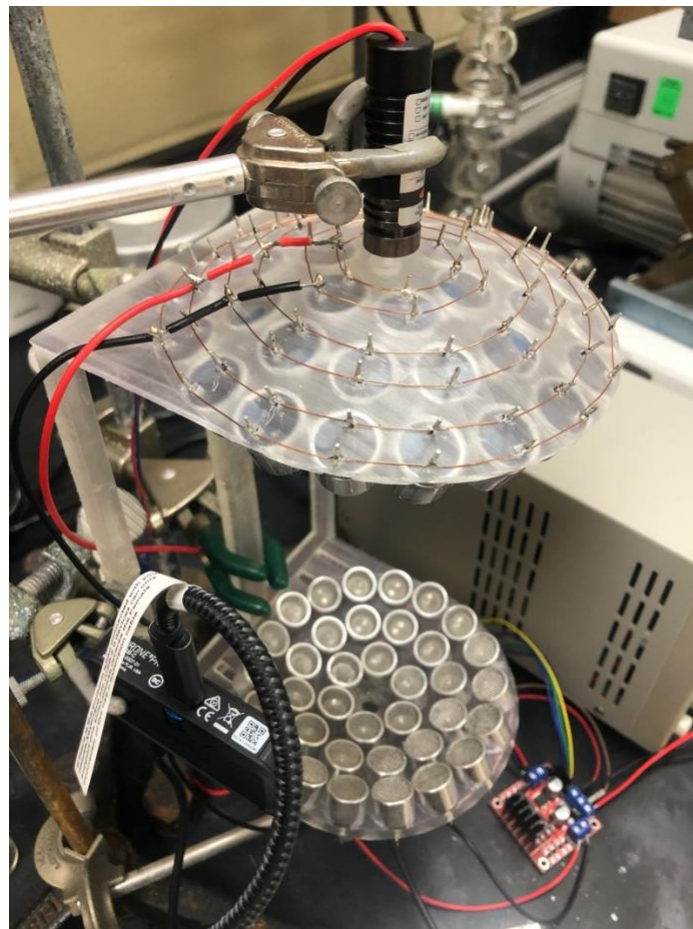

Figure 6. Wiring and set up for the BigLev.

III.   Acoustic Levitation

Before any droplets of resin can be levitated in the BigLev for data collection, it is important to check for laser alignment to ensure the lasers are hitting the top and bottom of the levitated bead. To do so, a tiny Styrofoam ball is levitated in one of the nodes after the power supply is turned on and the lasers are then plugged in to check the alignment. Adjustments were made as needed. After realigning the top and bottom lasers, the Styrofoam ball is removed and the BigLev is now ready for resin levitation. The first resin levitated was the clear commercial PMMA resin from formlabs; running the polymerization reaction and collecting data from this resin first allowed for a baseline to be established. In order to acoustically levitate a droplet of resin, the voltage on the power supply can range from 7V to 10V typically and the nodes must be identified. A thin black cloth that is made of an acoustically transparent material was placed on top of the bottom transducers of the BigLev in order to catch any droplets of resin that may fall from the nodes when attempting to levitate them. This fabric allows the transducers and base to remain clean from any resin that may affect the acoustic levitation. A small droplet of the PMMA resin was then gathered at the end of a pin to be transferred into the BigLev and placed in a node to levitate. In order to properly find a node, the pin with the resin is moved around in between the top and bottom transducers until a spot is found where the droplet begins to slightly warp, this warping is an indication of the location of a node. Once the node is found, the droplet of resin is gently dropped into the node where it should then levitate if done properly. If this

resin droplet is too large it may easily fall from the node, however, if the droplet is too small, the droplet may not pull away from the pin and drop into the node.
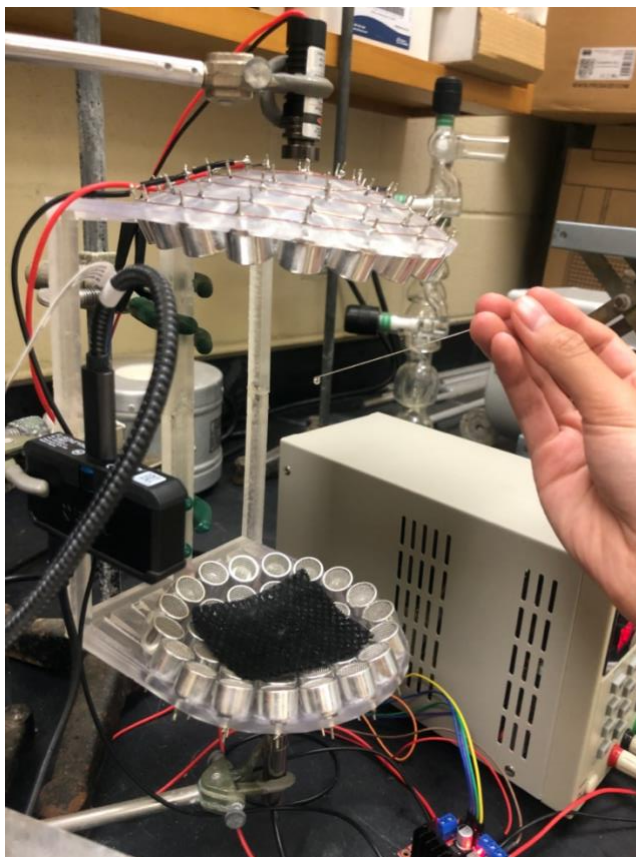
Figure 7. Levitating a droplet of commercial resin V4.

IV. Data Collection and Analysis

A Samsung Galaxy S7 edge phone and FLIR ONE Pro LT thermal camera were used to collect data on the FLIR Tools Mobile App using a USB to USB-C cord. The FLIR camera was attached to the same ring stand as the BigLev using clamps with the camera pointed toward the center of the acoustic field in between the top and bottom transducers. Once the droplet of resin was successfully levitating, the FLIR Tools Mobile App is opened to the "Instruments" tab and then the FLIR ONE Camera option was selected in order to access a live stream display of the

camera's visual field. A color gradient screen should appear indicating the difference in temperatures from the surroundings that the camera is picking up. After the sensor icon was selected from the bottom, the sensor was positioned in the center of the droplet shown on the screen. Where the center of the sensor is placed is where the camera will measure temperature.

To start recording, the red record button was pressed to then pull up options to name and choose file location. The session's name" was formatted with the date of data collection, the sample name, and the run number that was being recorded. The logging interval should be selected to 1 second with the "Record video from camera" box selected. After all of the settings and names were nominated, the "Save" button was selected to begin recording and collecting data. Before pressing "Save" it was important to make sure the thin black cloth is removed from the bottom transducers. A timer appears at the bottom right hand corner along with the temperature recording at the upper left-hand corner. After letting the recording run for 30 seconds, both the top and the bottom lasers were plugged in to turn on simultaneously. The recording is then allowed to run until it hits the 2 minute and 30 second mark where the red record button at the bottom of the screen is pressed to stop recording. While the droplet of resin was polymerizing and the temperature recorded, observations and logistics of the run were recorded in the lab notebook in the case that what occurred during a specific run needed to be referenced. While running the polymerization reaction, a UV protective shield and glasses were used to avoid direct contact of UV rays to the eyes for both bystanders and experimenter, respectively.
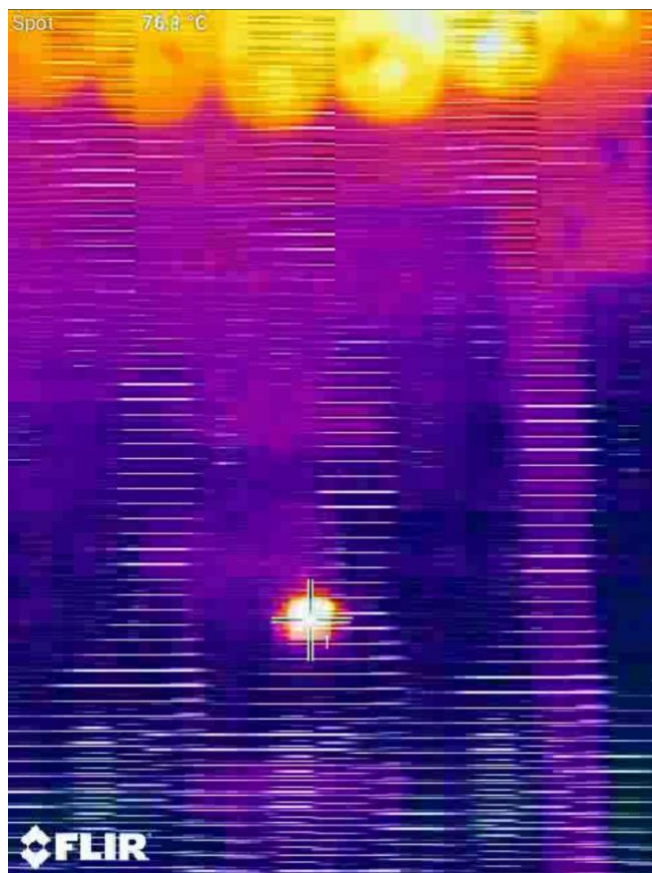
Figure 8. Example of phone screen when collecting data with the FLIR camera

After stopping the recording, both the lasers were unplugged to turn them off. The cloth was carefully placed back on top of the bottom transducers while the bead was still levitating in order to catch the polymerized bead in case it fell. Using a pair of tweezers, the fully hardened bead of PMMA was carefully removed and placed into the bottom of a glass scintillation vial with the cap labeled with the sample name and date. The bead was then labeled on the outside of the glass vial to differentiate between the different runs of that particular sample. Keeping up with the beads and corresponding data FLIR collected was necessary when running a differential scanning calorimetry (DSC) analysis and to further determine heat capacity using the change in temperature.

This process is repeated until five to ten beads/runs were collected per sample. After collecting the baseline data from the pure commercial PMMA, five to ten runs of data were collected from each of the following samples: 10% solution of recrystallized Phenylbis(2,4,6-trimethylbenzoyl) phosphine oxide, or BAPO, in methyl methacrylate, 10% mixture of recrystallized BAPO in distilled styrene, 10%, 20%, 30%, 40%, and 50% by weight solutions of each of the two ILs in the commercial pure PMMA resin. The two ILs tested in this research are (1-butyl-3-methylimidazolium bis(trifluorosulfonyl)imide ([Bmim][Tf2N]) and 1-ethyl-3-methylimidazoium acetate ([Emim][Ace]) shown in Figure 1 and Figure 2 respectively.

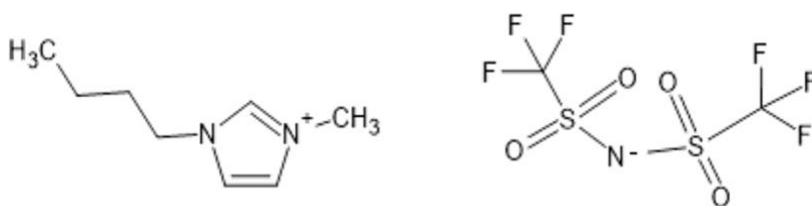

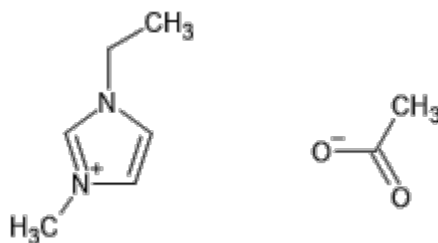Figure 9. Base structure for 1-butyl-3-methylimidazolium bis(trifluorosulfonyl)imide

Figure 10. Base structure for 1-ethyl-3-methylimidazoium acetate

The [Bmim][Tf2N] IL was synthesized in the lab according to literature procedures while the [Emim][Ace] IL was purchased.

V. Methyl Methacrylate, Styrene, and BAPO

Initially a small silica gel column was used to try to remove Hydroquinone, the inhibitor/stabilizer for methyl methacrylate. Next, standard microscale distillation was performed in attempt to also remove the inhibitor for MMA. Finally, a standard distillation with an Allihn condenser was used to try to remove p-tert-butylcatechol, the stabilizer in styrene. In order to remove any gases dissolved in the methyl methacrylate such as oxygen, three standard freeze-pump-thaw cycles were performed using a Schlenck line. The methyl methacrylate was capped and stored in the freezer until it was ready to be distilled. The methyl methacrylate was then distilled using standard procedure except the collection flask was cooled in a bath of liquid nitrogen preventing the flask with the MMA to have to be heated too extensively and causing thermal initiated polymerization. Standard recrystallization was performed to purify the initiator, BAPO. The recrystallized BAPO was then used to make a 10% solution by weight in the distilled methacrylate.
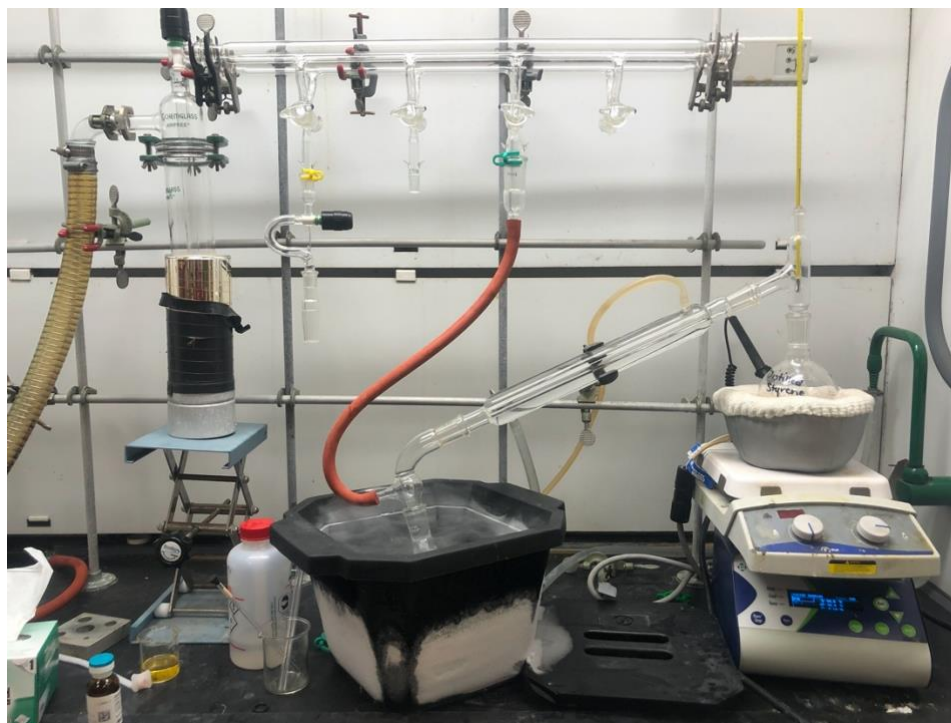
Figure 11. Set up for freeze-pump-thawing methyl methacrylate.

VI.   DSC Analysis

The thermogravimetric analysis, TGA 550, from TA Instruments was used to accurately

measure the mass of all of the polymerized beads, DSC pans and lids rather than using a lab

balance. The standard TA Instruments aluminum Tzero sample pans with the standard aluminum

Tzero lids were used to run analysis on the TA Instruments DSC 250 and the Tzero Press with

the hemispherical die. The experiment settings were consistent across all of the samples with the

procedure settings set as followed: Data Off, Ramp for 5°C/min to 100C, Isothermal for 5

minutes, Ramp 2°C/min to 0°C, Isothermal for 5 minutes, Modulate T 1°C for 60 seconds,

Isothermal for 5 minutes, Data On, Ramp 2°C/min to 100°C, Isothermal for 5 minutes, Event 1

Off, Data Off. In order to retrieve and process the DSC data, the Reversing Heat Capacity

(Normalized) Variable was added to a second y axis with the data table data ranging only from

20°C to 80°C; it was then exported as a CSV file to be used in heat capacity and heat of polymerization calculations.
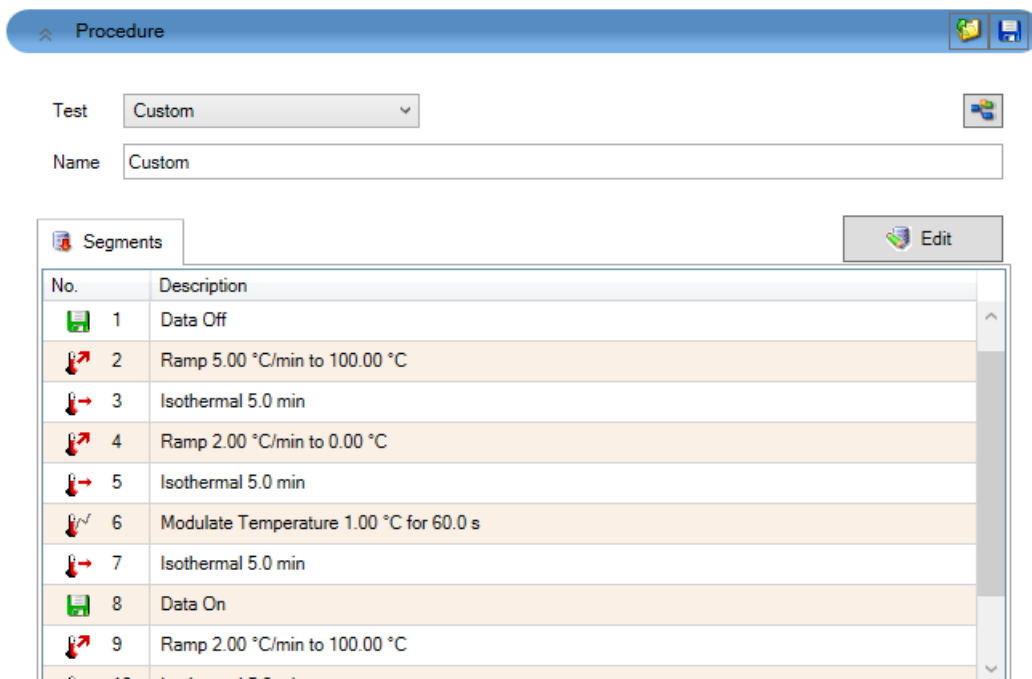
Figure 12. Example of what DSC settings should look like before running a sample.

VII.   Calculations

The first calculation necessary established the average temperature for the baseline of each run, in order to calculate ΔT. Once the temperature has returned to a steady baseline, all of those points are averaged together to get a number that will then be subtracted from the max temperature of that run to give ΔT. To calculate ΔH, the heat capacity was simply multiplied with the ΔT found for each run.

$$\Delta H = \Delta T * Cp$$

In order to calculate the propagation of error for ΔH the following equation was used:

$$\delta_{\Delta H}{}^2 = (\sigma_{\Delta T})^2 * (Cp)^2 + (\sigma_{Cp})^2 * (\Delta T)^2$$

CHAPTER 5

RESULTS AND DISCUSSION

I.   FLIR Data

The typical data that was collected from the FLIR camera is shown in the graph below with the temperature recorded every second for 2 minutes and 30 seconds. The baseline is considered to be where the temperature drops back down to a relatively steady temperature, which is around 38°C for the specific run shown.
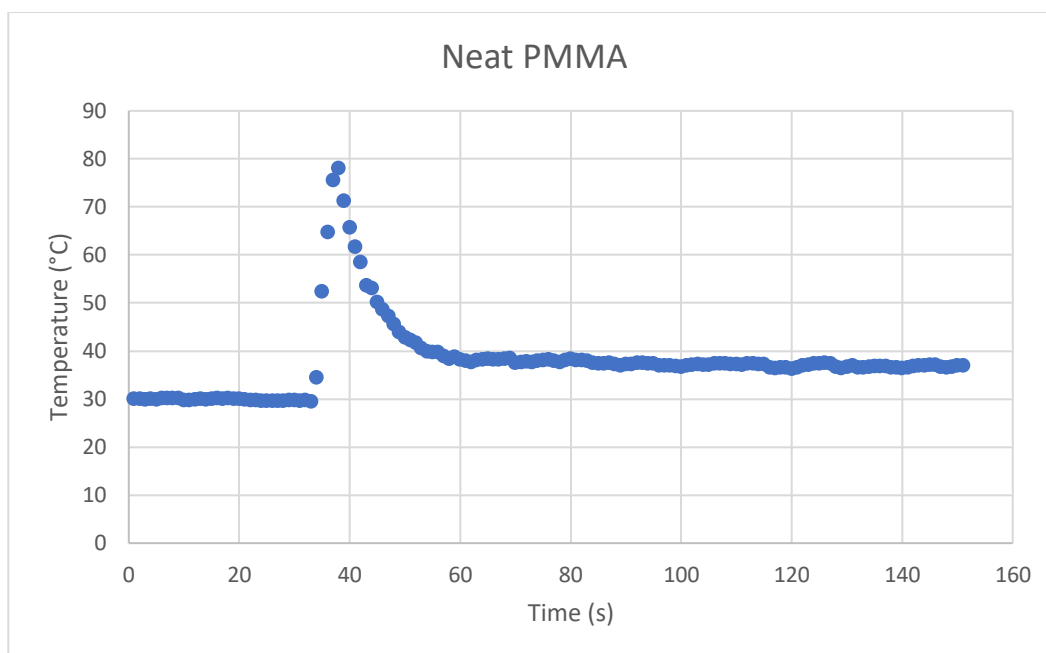

Figure 13. Graph of raw data taken from FLIR camera for pure PMMA

Since multiple runs (typically 5) were collected for each percentage, the ΔTs for all the runs were averaged together to give an average ΔT for each percentage as shown in the graph below

for both [Bmim][Tf$_2$N] and [Emim][Ace]. For [Bmim][Tf$_2$N], a general downward trend is

observed except for the 40% sample which spikes up rather than following the trend. Meanwhile

for [Emim][Ace], a consistent downward trend is observed but the ΔT drops much farther going

from 0% to 10% IL in PMMA than in [Bmim][Tf$_2$N]. The ΔT drops approximately 10 degrees

for [Bmim][Tf$_2$N] but the ΔT decreases over double that amount for [Emim][Ace] and continues
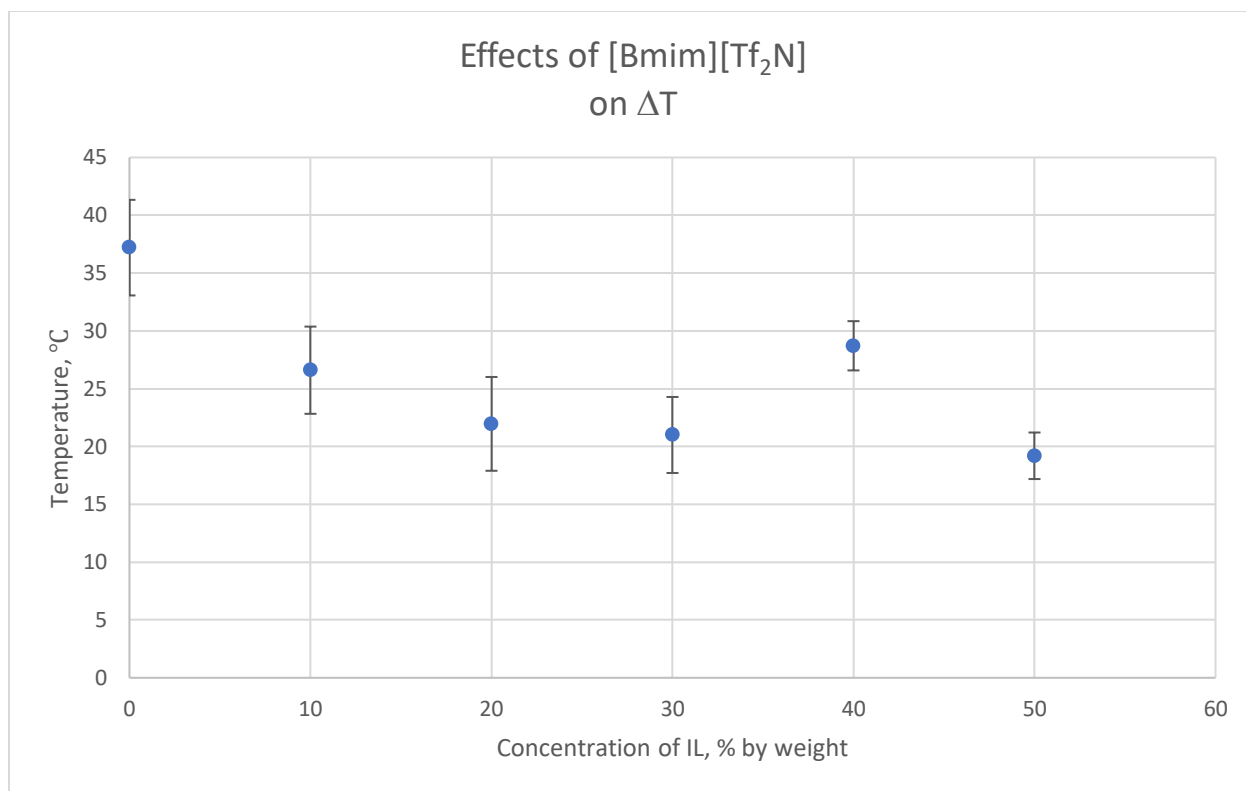
to decrease.

Figure 14. Graph of the average ΔTs for each % of [Bmim][Tf$_2$N] in PMMA.
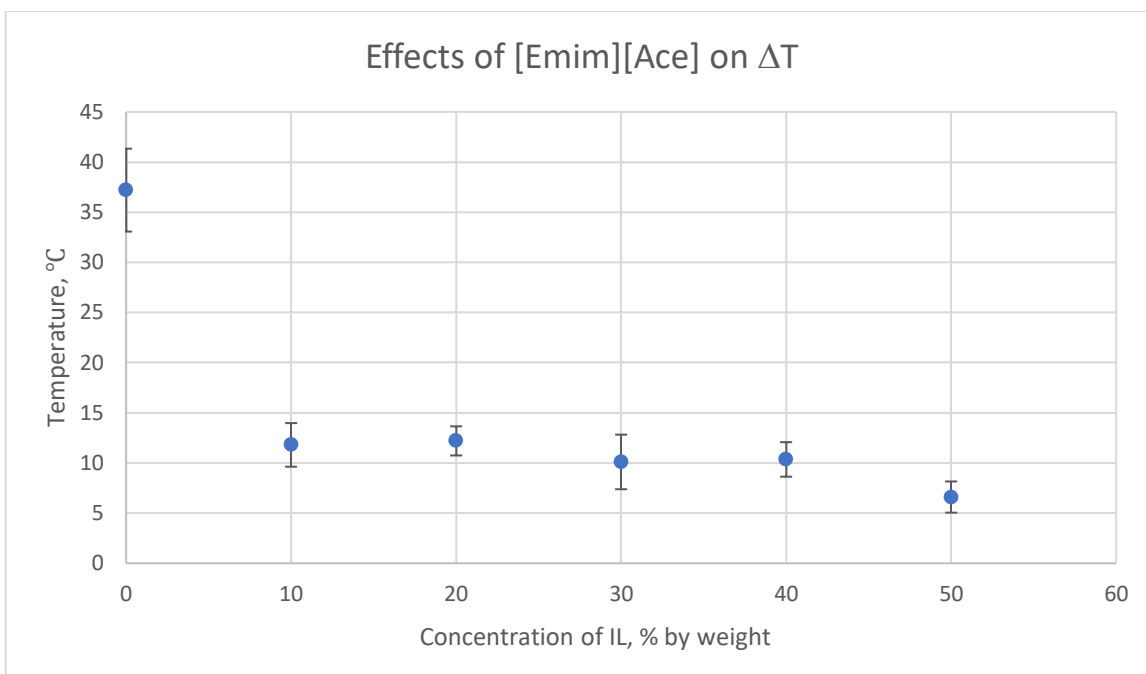
Figure 15. Graph of the average ΔTs for each % of [Emim][Ace] in PMMA.

A possible explanation for the peak in the 40% of the [Bmim][Tf$_2$N] could be due to a certain anion interaction of the IL with the polymer in comparison to the [Emim][Ace]. With [Emim][Ace], the acetate anion is much smaller than the bistrifylimide anion of the [Bmim][Tf$_2$N] which could allow it to more easily interact with the polymer, resulting in significantly more conformation possibilities. On the other hand, since the bistrifylimide is a much bulkier anion, that peak in the 40% might be depicting a critical concentration where enough IL is being introduced to where it is forming pockets of self-aggregates rather than interacting with the methyl methacrylate as a solvent. As a result, the peak in temperature could reflect a more complete polymerization of the monomer and thus accounting for the temperature spike. In the 0-30% range, the expected decrease in ΔT is evident due to the concentration of IL; it may not be enough to start forming those pockets of itself yet but acts as solvent. Therefore,

the more solvent added, the more dilute the methyl methacrylate becomes and, in return, the temperature is dropping from lower extent of reaction of the monomer. This biphasic behavior is not apparent with the [Emim][Ace] shown in the ΔT data which could be in part because it has an easier time interacting with the monomer and acting as a solvent that it does not form those self-aggregates as speculated with the [Bmim][Tf$_2$N].

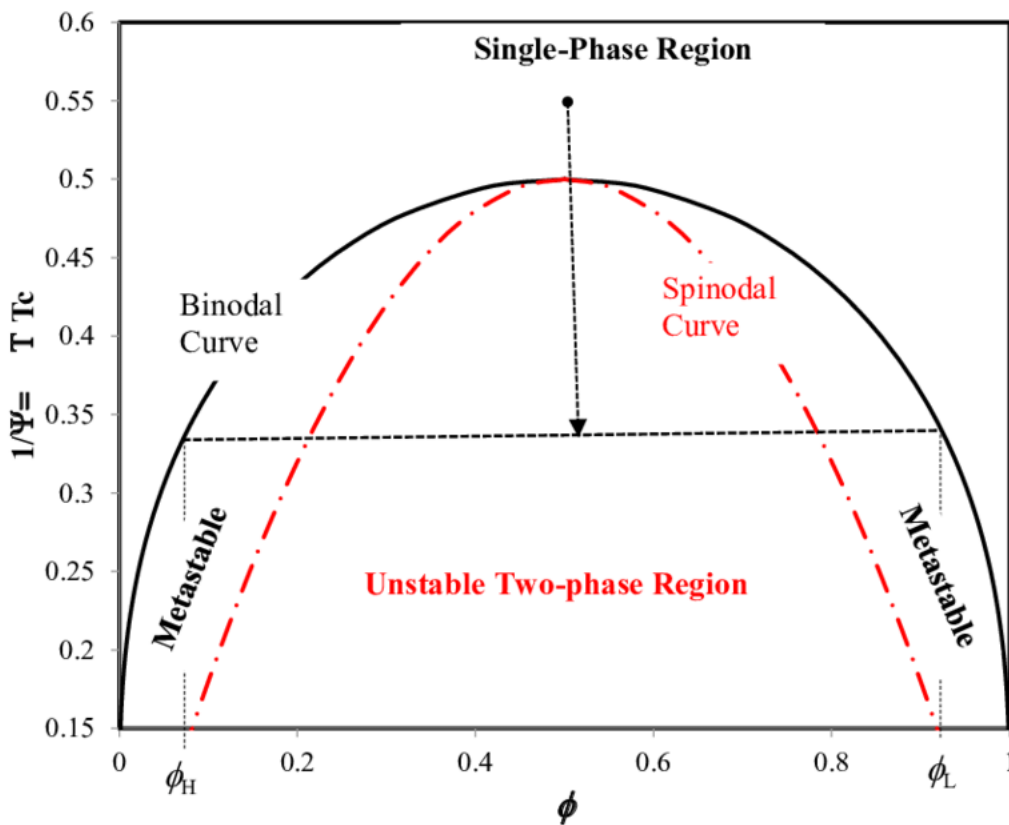Figure 16. Example of a generic UCST graph.[20]

A more visual explanation of the [Bmim][Tf$_2$N] pockets in the methyl methacrylate at the critical concentration is shown in the graph above. The 0-30% concentration of IL could fall outside of the binodal curve in the single-phase region which is consistent with the IL acting as solvent and not interacting or affecting the polymerization. However, when a critical

concentration is reached (around 40% for [Bmim][Tf₂N]), this could be representative of crossing the binodal curve into the metastable region or even the unstable two-phase region where there is an uneven distribution of monomer and IL in solution. Finally, what could explain the drop in ΔT again at 50% is crossing back over the other side of the binodal curve back into the single-phase region where there is now a significant amount of IL to act as solvent again. It is also important to note that the graph shown above is an example of an upper critical solution temperature (UCST) phase diagram. However, in actuality, what is being observed in this experiment could also be better represented in a lower critical solution temperature (LCST) phase diagram. Currently, it is unknown what the exact curve is for this project but could be found experimentally by using something like the cloud point technique. Regardless, the theory behind the binodal curve remains the same in looking at how varying concentrations could affect phase separation.

II.   DSC Data

The graph shown below is a standard plot given from the DSC250 displaying Heat Flow and Reversing Heat Capacity but is not corrected for cell constant. Since this instrument did not correct for cell constant and needed to be corrected by subtracting the change in Cp due to the temperature change in the cell was subtracted from the TRIOS modulated Cp data in Origin software to get a corrected Cp which is depicted by the relatively flat orange line below. The flat line is more representative of the actual Cp because heat capacity should not change with temperature. The average of the corrected line was calculated in order to get the corrected Cp value for each data run. The equation for the correction calculation is shown below.

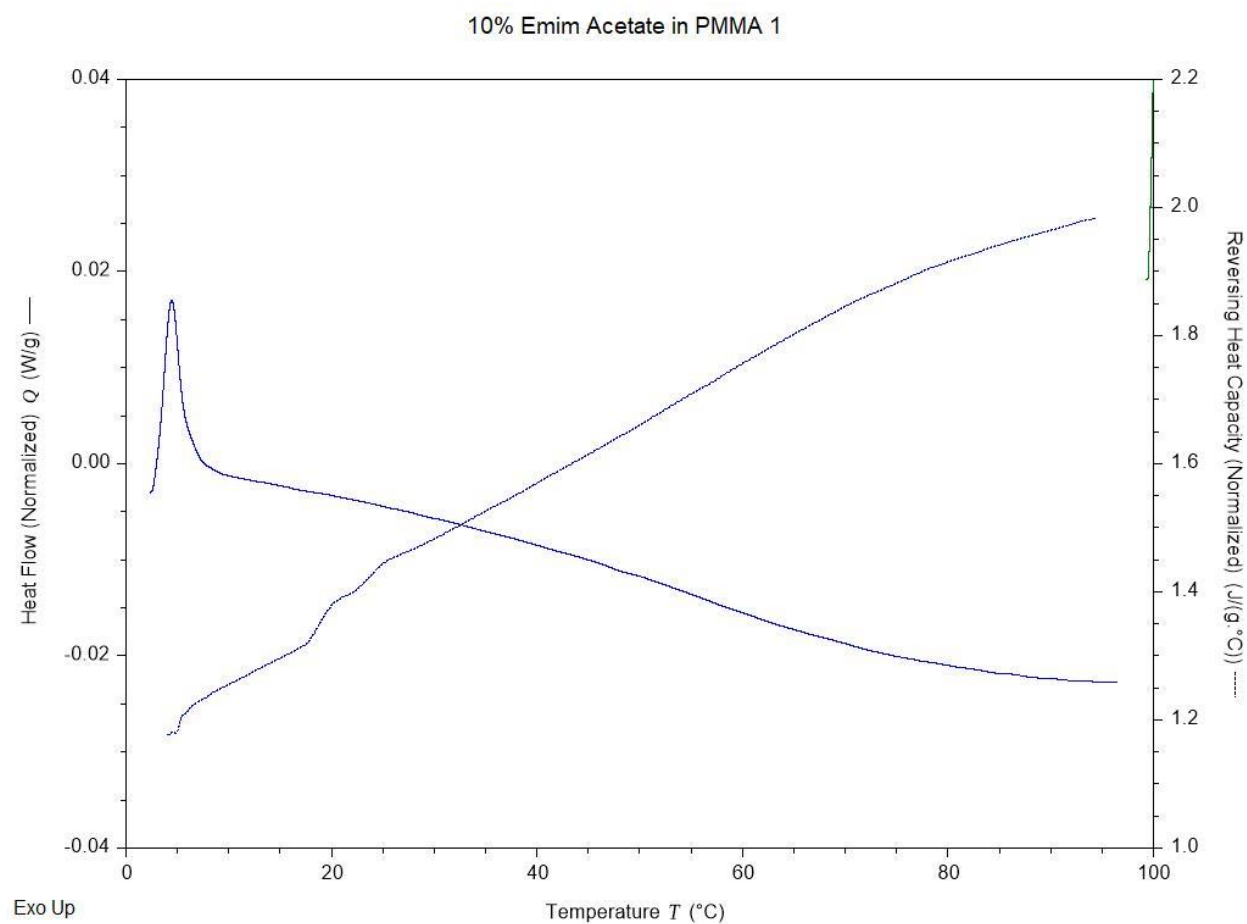$$Corrected\ Cp = Cp - ((\Delta T) * \text{slope of Cp})$$

Figure 17. Plot of average ΔTs for each % of [Bmim][Tf$_2$N] in PMMA given by DSC250.
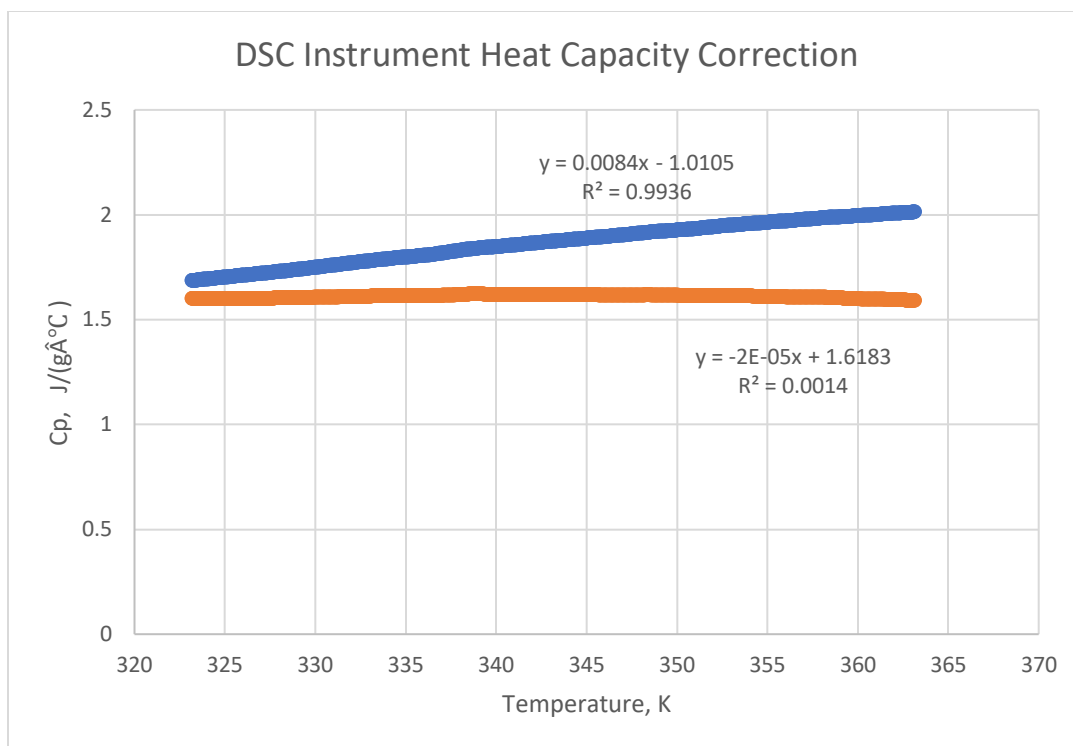
Figure 18. Graph of modulated Cp values from DSC and corrections.

The two graphs below show how the corrected Cp values were affected by the different increases of the IL. The Cp values for [Bmim][Tf$_2$N] show a downward trend in the 0-20% but then a spike is observed at 30% with the Cp values displaying a similar downward trend. The opposite is seen however for [Emim][Ace] where the Cp values depict an overall upward trend. If heat capacity is the measure of the amount of heat that a molecule can store before changing temperature then the higher the heat capacity, the more possibilities of the molecule rotation and vibration before the molecules just simply moves where temperature is the average translational motion or average kinetic energy of the polymer. By introducing anions that are coordinating with the polymer, the possibilities for more correlated rotations and vibrations suddenly increases in comparison with the polymer on its own. Since the acetate anion should more easily interact with the monomer than the bistriflimide anion, this could potentially explain why the

heat capacity for the [Emim][Ace] is increasing but the [Bmim][Tf2N] is showing decreases. The Cp values for [Emim][Ace] are also higher in comparison with the Cp values of [Bmim][Tf2N] which is consistent with this theory of greater anion-polymer correlation.
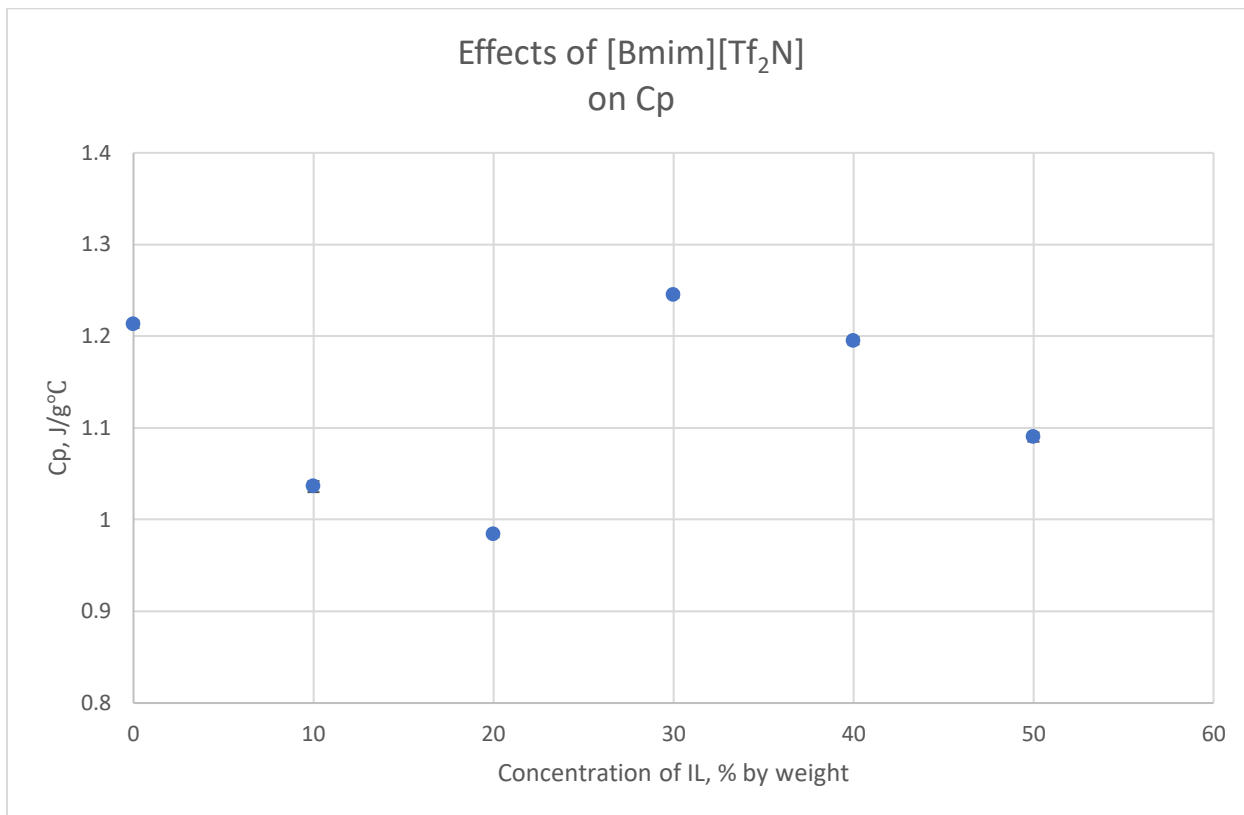

Figure 19. Graph of average Cp values for each % of [Bmim][Tf2N] in PMMA
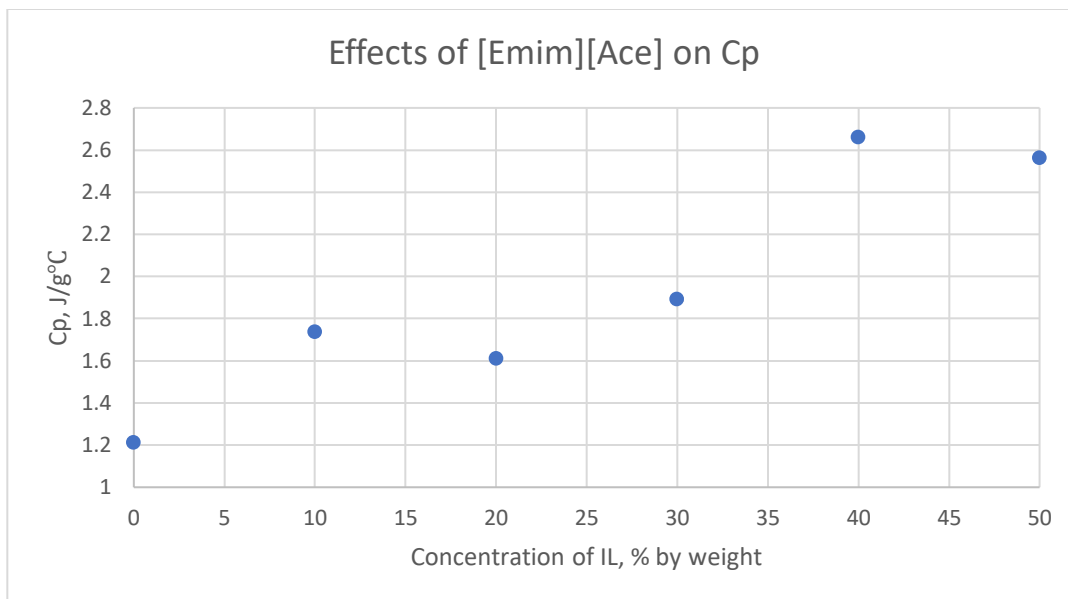
Figure 20. Graph of average Cp values for each % of [Emim][Ace] in PMMA

III. Enthalpy

The heat of polymerization for the different IL percent loadings in PMMA is shown in the two graphs below. In Figure 21, the enthalpy of the [Bmim][Tf$_2$N] shows a downward trend and then peaks at the 30% and 40% concentration before going back down at the 50% loading. This trend is consistent with the ΔT trend as well as the trend for the heat capacity. It is evident that some interaction is occurring with this IL at the 30-40% loading which, as discussed before, is probably due to the critical concentration being reached and as a result has the same effect on the heat of polymerization.

Figure 21. Graph of calculated ΔH values for each % of [Bmim][Tf₂N] in PMMA

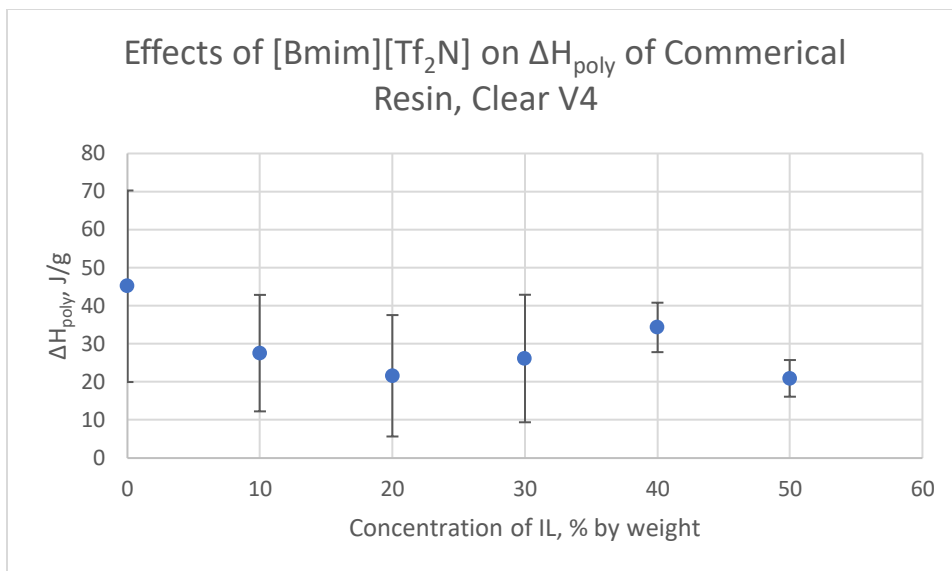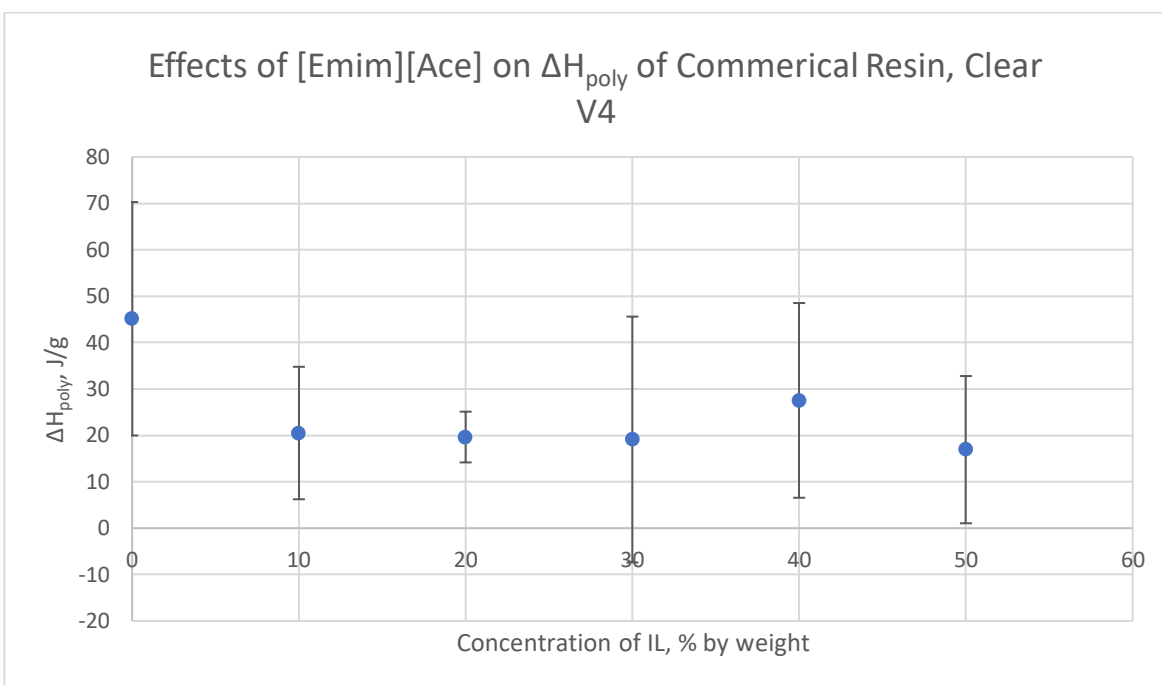Figure 22. Graph of calculated ΔH values for each % of [Emim][Ace] in PMMA

The ΔH trend for [Emim][Ace] (Figure 22) decreases initially but almost levels off until the 40% loading spike that is similarly seen in the [Bmim][Tf2N] and then it drops back off again at the 50% concentration. This general trend is more consistent with the ΔT data in comparison with the Cp data for [Emim][Ace]. This could indicate that ΔT plays a greater impact role on the determination of enthalpy for this reaction. It appears that the thermal effects are greater on heat of polymerization than the kinetic effects since the graph of the ΔT is more similar to the trend from the enthalpy graph than the Cp trend is with the enthalpy. In other words, this reaction is more heavily temperature dependent.

The FLIR data is showing the energy that is given off by temperature change during the polymerization reaction while the heat capacity data from the DSC shows how much energy the polymer can absorb. By multiplying these two values together, this allows for the calculation of ΔH and for a more wholistic picture of what is occurring. Only having the ΔT or only the heat capacity would be insufficient to accurately display what is happening in the reaction. It is necessary to know both the heat given off from the reaction as well as the amount of heat the polymer can absorb (Cp) to fully understand what is occurring. The ΔT data ultimately determines if the reaction is exothermic or endothermic, while the Cp is responsible for the magnitude in the ΔH. For this experiment in particular, since the ΔT values were positive, the reaction was exothermic.

IV.   10% Recrystallized BAPO in Distilled MMA

The graph below shows a much slower rate of polymerization of this recrystallized BAPO in distilled methyl methacrylate solution in comparison with the commercial PMMA resin. The trend is generally the same consisting of the temperature peaking and then returning to baseline

with the exception that there appears to be a step-like increase in the temperature rather than an almost vertical peak shown in other runs with commercial resin. Granted, due to poor temporal resolution, it is uncertain of what is exactly happening at those vertical peaks simply because the camera cannot capture what is happening as fast as the reaction is actually happening. The average ΔT of these runs were 20.93 °C with a standard deviation of 2.56. The calculated Cp value was 0.68 J/g°C which in turn resulted in the ΔH to be 14.23 J/g. These values are relatively similar to the commercial PMMA resin which is a good indicator that the lab-made version is comparable.
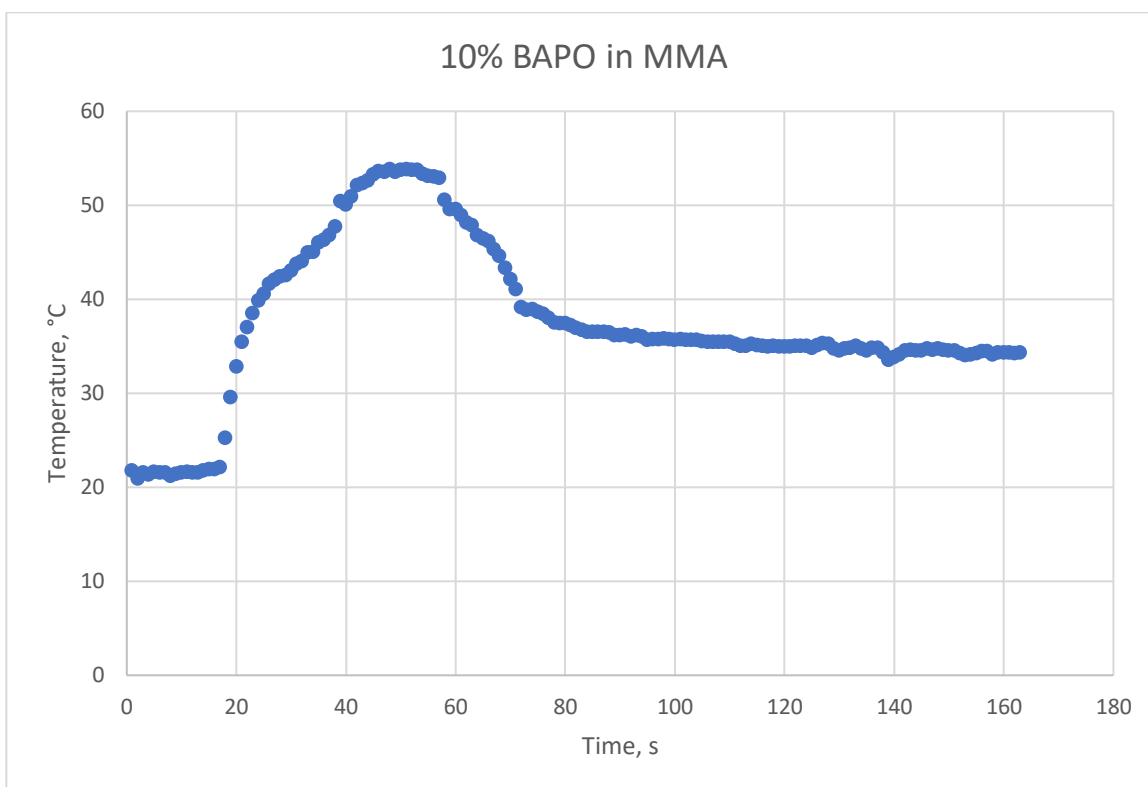

Figure 23. Graph of temperatures recorded from FLIR camera for the polymerization of BAPO in MMA

V. Future Work

Future work for this project includes further experimentation with other polymers such as polystyrene and polyacrylonitrile in a similar manner as PMMA to determine heat capacity and heat of polymerization. Improvements that could be made to the data collection process are purchasing a new FLIR camera with better temporal resolution to ensure that the actual maximum temperature is being recorded and not lost due to lack of more precise equipment. The temporal resolution is currently 8Hz or capturing 8 frames per sec currently. Also, in order to keep all of the data consistent, the BigLev and lasers could be mounted to a more permanent structure or base so there is no discrepancy of how far the lasers are or how centered the lasers are on the droplet in case the set-up is accidentally bumped or moved; if the lasers are more centered on the droplet in one sample run versus being off centered on another has an effect on the polymerization reaction thus creating an issue with standardization amongst all of the runs. By making some modifications to the BigLev laser setup, this could eliminate possible variables that might interfere with getting consistent temperature data being recorded from the FLIR camera. Additionally, thermogravimetric analysis (TGA) could be run to determine effects of the ILs on the thermal stability in addition to the how they affect heat capacity. More ILs could be tested in the same regard to see the varying effects that each IL has on the heat of polymerization and if there are any trends found between similarly structured ILs.

CHAPTER 6

CONCLUSION

The effects of two different ILs in the polymerization of PMMA were successfully observed via acoustic levitation and thermal imaging from a FLIR camera. The ILs [Bmim][Tf$_2$N] and [Emim][Ace] were added to commercial resin, clear V4 to create 10%, 20%, 30%, 40%, and 50% solutions by weight for each of the two ILs which droplets were then levitated and polymerized in the BigLev. Preliminary FLIR data allowed for the ΔT to be calculated which revealed a potential critical concentration in which the [Bmim][Tf$_2$N] is segregating but is not the case for the [Emim][Ace]. The heat capacities found from DSC showed opposite trends in the two ILs with the [Bmim][Tf$_2$N] Cp values generally decreasing while the [Emim][Ace] Cp values were generally increasing with increasing concentration of IL. While it was predicted that the IL acts only as a solvent diluting the methyl methacrylate, the data indicates that interactions are happening but in different ways depending on the IL, specifically their anion. If the ILs only act as a solvent a steady decrease in the heat of polymerization should be seen with the increase of IL concentration, however, this was not shown to be the case. From current observations it is speculated that the polymer-anion interaction is greater with the acetate than the bistriflimide anion. Future work includes improving the acoustic levitation set up to produce more standard results as well as experimentally finding the potential binodal curve in which the phase shift is occurring.

REFERENCES

(1)   Fredlake, C. P.; Crosthwaite, J. M.; Hert, D. G.; Aki, S. N. V. K.; Brennecke, J. F. Thermophysical Properties of Imidazolium-Based Ionic Liquids. *J. Chem. Eng. Data* **2004**, *49* (4), 954–964. https://doi.org/10.1021/je034261a.

(2)   Singh, S. K.; Savoy, A. W. Ionic Liquids Synthesis and Applications: An Overview. *J. Mol. Liq.* **2020**, *297*, 112038. https://doi.org/10.1016/j.molliq.2019.112038.

(3)   E. Visser, A.; P. Swatloski, R.; Matthew Reichert, W.; Mayton, R.; Sheff, S.; Wierzbicki, A.; James H. Davis, J.; D. Rogers, R. Task-Specific Ionic Liquids for the Extraction of Metal Ions from Aqueous Solutions. *Chem. Commun.* **2001**, *0* (1), 135–136. https://doi.org/10.1039/B008041L.

(4)   G. Huddleston, J.; E. Visser, A.; Matthew Reichert, W.; D. Willauer, H.; A. Broker, G.; D. Rogers, R. Characterization and Comparison of Hydrophilic and Hydrophobic Room Temperature Ionic Liquids Incorporating the Imidazolium Cation. *Green Chem.* **2001**, *3* (4), 156–164. https://doi.org/10.1039/B103275P.

(5)   Li, X.; Zhao, D.; Fei, Z.; Wang, L. Applications of Functionalized Ionic Liquids. *Sci. China Ser. B Chem.* **2006**, *49* (5), 385–401. https://doi.org/10.1007/s11426-006-2020-y.

(6)   Scott, M. P.; Rahman, M.; Brazel, C. S. Application of Ionic Liquids as Low-Volatility Plasticizers for PMMA. *Eur. Polym. J.* **2003**, *39* (10), 1947–1953. https://doi.org/10.1016/S0014-3057(03)00129-0.

(7)   Kubisa, P. Application of Ionic Liquids as Solvents for Polymerization Processes. *Prog. Polym. Sci.* **2004**, *29* (1), 3–12. https://doi.org/10.1016/j.progpolymsci.2003.10.002.

(8)   Etheredge, A. W.; Ellett, T. R.; Poole, G. M.; Reichert, W. M. Plasticization of PMMA Components Using Imidazolium-Based Ionic Liquids in Stereolithography Additive Manufacturing. *ECS Trans.* **2018**, *86* (14), 239. https://doi.org/10.1149/08614.0239ecst.

(9)   Mishra, V.; Kumar, R. Living Radical Polymerization-A Review. October 31, 2012.

(10)   Hadjichristidis, N.; Iatrou, H.; Pispas, S.; Pitsikalis, M. Anionic Polymerization: High Vacuum Techniques. *J. Polym. Sci. Part Polym. Chem.* **2000**, *38* (18), 3211–3234. https://doi.org/10.1002/1099-0518(20000915)38:18<3211::AID-POLA10>3.0.CO;2-L.

(11)   Hirao, A.; Goseki, R.; Ishizone, T. Advances in Living Anionic Polymerization: From Functional Monomers, Polymerization Systems, to Macromolecular Architectures. *Macromolecules* **2014**, *47* (6), 1883–1905. https://doi.org/10.1021/ma401175m.

(12)   Bhudolia, S. K.; Perrotey, P.; Joshi, S. C. Optimizing Polymer Infusion Process for Thin Ply Textile Composites with Novel Matrix System. *Materials* **2017**, *10* (3). https://doi.org/10.3390/ma10030293.

(13)   Bisht, H. S.; Chatterjee, A. K. Living Free-Radical Polymerization—a Review. *J. Macromol. Sci. Part C* **2001**, *41* (3), 139–173. https://doi.org/10.1081/MC-100107774.

(14)   Yagci, Y.; Jockusch, S.; Turro, N. J. Photoinitiated Polymerization: Advances, Challenges, and Opportunities. *Macromolecules* **2010**, *43* (15), 6245–6260. https://doi.org/10.1021/ma1007545.

(15)   Andrade, M. A. B.; Marzo, A.; Adamowski, J. C. Acoustic Levitation in Mid-Air: Recent Advances, Challenges, and Future Perspectives. *Appl. Phys. Lett.* **2020**, *116* (25), 250501. https://doi.org/10.1063/5.0012660.

(16)   Santesson, S.; Nilsson, S. Airborne Chemistry: Acoustic Levitation in Chemical Analysis. *Anal. Bioanal. Chem.* **2004**, *378* (7), 1704–1709. https://doi.org/10.1007/s00216-003-2403-2.

(17) Schenk, J.; Panne, U.; Albrecht, M. Interaction of Levitated Ionic Liquid Droplets with Water. *J. Phys. Chem. B* **2012**, *116* (48), 14171–14177. https://doi.org/10.1021/jp309661p.

(18) Fontana, S.; Moeller, D.; Liu, I.; Robins, K. Acoustic Levitation: A Theoretical Exploration. 11.

(19) Marzo, A.; Barnes, A.; Drinkwater, B. W. TinyLev: A Multi-Emitter Single-Axis Acoustic Levitator. *Rev. Sci. Instrum.* **2017**, *88* (8), 085105. https://doi.org/10.1063/1.4989995.

(20) Ullmann, A.; Poesio, P.; Brauner, N. Enhancing Heat Transfer Rates by Inducing Liquid-Liquid Phase Separation: Applications and Modelling. *Interfacial Phenom. Heat Transf.* **2015**, *3*. https://doi.org/10.1615/InterfacPhenomHeatTransfer.2015012506.